Inertial migration of an elastic capsule in a Poiseuille flow

Soo Jai Shin and Hyung Jin Sung*

Department of Mechanical Engineering, KAIST, 291 Daehak-ro, Yuseong-gu, Daejeon, 305-701, Korea

(Received 28 October 2010; revised manuscript received 9 February 2011; published 28 April 2011)

The inertial migration of a two-dimensional elastic capsule in a Poiseuille flow was studied over the Reynolds number range $1 \leqslant \mathrm{Re} \leqslant 100$. The lateral migration velocity, slip velocity, and the deformation and inclination angle of the capsule were investigated by varying the lateral position, Reynolds number, capsule-to-channel size ratio (λ), membrane stretching coefficient (ϕ), and membrane bending coefficient (γ). During the initial transient motion, the lateral migration velocity increased with increasing Re and λ, but decreased with increases in ϕ,γ, and the lateral distance from the wall. On the other hand, the deformation of the capsule increased and the inclination angle became smaller as Re, ϕ, γ, and the distance from the wall decreased. The initial behavior of the capsule was influenced by variation in the initial lateral position (y_0), but the equilibrium position of the capsule was not affected by such variation. The balance between the wall effect and the shear gradient effect determined the equilibrium position. As Re increased, the equilibrium position initially shifted closer to the wall and then moved toward the channel center. A peak in the equilibrium position was observed near $\mathrm{Re} = 30$ for $\lambda = 0.1$, and the peak shifted to higher Re as λ increased. Depending on the lateral migration velocity, the equilibrium position moved toward the centerline for larger λ, but moved toward the wall for larger ϕ and γ.

DOI: 10.1103/PhysRevE.83.046321 PACS number(s): 47.63.−b, 47.11.−j, 87.16.A−, 87.16.D−

I. INTRODUCTION

Capsules consisting of a liquid drop enclosed by a thin deformable membrane are often employed as models for deformable particles such as biological cells and vesicles [1,2]. The mechanics of an elastic capsule immersed in a viscous flow has been studied by many researchers in biology, bioengineering, and chemical engineering. Capsule mechanics is particularly important in medical and industrial applications that use it for cell and particle manipulation. To develop various capsule products or to facilitate advanced control of capsules, the principles of capsule mechanics are widely used in the pharmaceutical, cosmetic, biomedical, and biochemical industries [3,4].

Capsule mechanics has been studied using both theoretical and experimental techniques. A theory of the small deformations of elastic capsules with thin and linear viscoelastic membranes was developed for a simple shear flow by Barthès-Biesel [5]. Rao *et al.* [6] solved the large deformation of two-dimensional (2D) capsules in a shear flow by using a series expansion technique. Chang and Olbricht [7] investigated experimentally the deformation of an artificial capsule freely suspended in a circular Couette flow driven by two counterrotating concentric cylinders. Walter *et al.* [8] obtained experimental results for the mechanical properties of an elastic capsule in a simple shear flow. Numerical studies of capsule mechanics have begun to be performed relatively recently. Ramanujan and Pozrikidis [9] studied a liquid capsule in a simple shear flow for vanishing Reynolds numbers by using a boundary-element method to investigate the effects of fluid viscosity on capsule deformation. In particular, Pozrikidis [1] modeled red blood cells as capsules with various initial shapes and membrane properties. Sui *et al.* [10] investigated the flow-induced deformation of an elastic capsule in a simple shear flow by varying the membrane bending stiffness. Recently, Sui *et al.* [11] extended a hybrid method based on the lattice Boltzmann method to investigate the behavior of a three-dimensional (3D) capsule.

However, in most of the studies of wall-bounded shear flow mentioned above, capsule migration was not considered. Chan and Leal [12] investigated the lateral migration of a sphere in a Poiseuille flow by using a fluid drop model and a perturbation expansion method. Doddi and Bagchi [13] studied capsule migration under large deformation in a channel flow with small fluid inertia. Ma *et al.* [14] investigated the initial motion of a 2D capsule in a microchannel, and the effects on capsule mechanics of elasticity, initial capsule shape, and initial capsule position were analyzed. In all these studies, however, the inertial effect was not considered. Recently, the inertial effect on the migration of particles in microscale flows has received significant attention [3,4,15]. Di Carlo [16] suggested a promising practical application of the inertial lift forces intrinsic to particle motions in particle separation and bioparticle focusing. Precise cell and particle manipulations can be achieved using the inertial lift forces to particle migrations in a channel flow. Fundamental studies of the inertial migration of particles on a macroscale have been reported by Segré and Silberberg [17], who demonstrated that a spherical particle in a pipe flow migrates to a specific equilibrium position and that particle migration across the streamline originates from the presence of fluid inertia. A number of theoretical and numerical methods have been developed to interpret these nonintuitive results [18–20]. Although the inertial migration of particles in Poiseuille flows has been investigated, most studies have focused on rigid particle motion and little research into the inertial migration of elastic particles has been performed.

In the present study, to analyze the effects of fluid inertia on the transverse movements of elastic particles, the inertial migration of an elastic capsule in a Poiseuille flow was investigated numerically in the Reynolds number range $1 \leqslant \mathrm{Re} \leqslant 100$. We used the immersed boundary (IB) method, which has previously been used to solve fluid-flexible body

*hjsung@kaist.ac.kr

interaction problems [21–23]. The flow field was calculated in a Eulerian grid system with a Navier-Stokes solver that employs the fractional step method and a staggered Cartesian grid. The capsule behavior was determined by solving the structural equation of motion in a Lagrangian coordinate with a uniform grid on the membrane. The capsule membrane was assumed to obey linear elastic rules. The fluid motion and the capsule motion were solved independently and their interaction was formulated in terms of momentum forcing. The lateral migration velocity, slip velocity, deformation, and the inclination angle of the elastic capsule were examined by varying the initial lateral position (y_0), Reynolds number, capsule-to-channel size ratio (λ), membrane stretching coefficient (ϕ), and membrane bending coefficient (γ). The effects of varying these parameters on the equilibrium position and tank-treading motion were also analyzed.

II. PROBLEM FORMULATION

A schematic diagram of the flow configuration of a circular elastic capsule moving in a Poiseuille flow is shown in Fig. 1. The half-channel height and the radius of the capsule are H and a, respectively. The capsule-to-channel size ratio is $\lambda = a/\mathrm{H}$ and the initial position of the capsule centroid is denoted by (x_0, y_0). Initially, an undisturbed parabolic velocity profile was imposed

$$u(y) = U_{\mathrm{m}}\left(1 - \frac{y^2}{\mathrm{H}^2}\right) \quad \text{for } -\mathrm{H} \leqslant y \leqslant \mathrm{H}, \tag{1}$$

where U_m is the maximum velocity at the centerline of the channel. The periodic boundary condition was adopted in the x direction and the length of the channel is L. In this approach, we actually consider the motion of an array of capsules, rather than of a perfectly isolated capsule, because of the periodic boundary condition in the x direction. It has been shown that the intercapsule distance (or channel length L) influences the motion of such capsules [13]. In the present study, the channel length was set at $\mathrm{L} = 8\mathrm{H}$, so the hydrodynamic interactions between the capsules almost vanish.

The capsule has an elastic membrane on the boundary Γ when the Lagrangian coordinate (s) is used. The capsule is immersed in a fluid domain Ω that is described in Eulerian

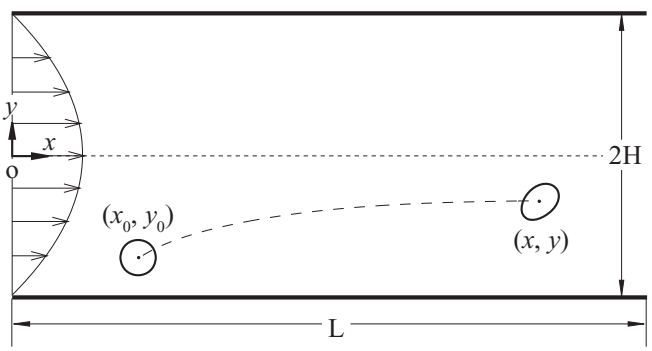

FIG. 1. Schematic diagram of an elastic capsule in a Poiseuille flow.

coordinates ($\mathbf{x}$). The incompressible viscous flow is governed by the Navier-Stokes equations and the continuity equation

$$\rho_0\left(\frac{\partial \mathbf{u}}{\partial t} + \mathbf{u}\cdot\nabla\mathbf{u}\right) = -\nabla p + \mu\nabla^2\mathbf{u} + \mathbf{f}, \tag{2}$$

$$\nabla\cdot\mathbf{u} = 0, \tag{3}$$

where $\mathbf{u}$ is the velocity vector, p is the pressure, ρ_0 is the fluid density, μ is the dynamic viscosity of the fluid, and $\mathbf{f}$ is the Eulerian forcing acting on the immersed boundary (IB), as constrained by the no-slip boundary condition. The structural equation of motion of the elastic capsule can be expressed as

$$\rho_1\frac{\partial^2\mathbf{X}}{\partial t^2} = \frac{\partial}{\partial s}\left(\phi\left(\left|\frac{\partial\mathbf{X}}{\partial s}\right| - 1\right)\frac{\partial\mathbf{X}}{\partial s}\Big/\left|\frac{\partial\mathbf{X}}{\partial s}\right|\right) - \frac{\partial^2}{\partial s^2}\left(\gamma\,(\kappa-\kappa_0)\frac{\partial^2\mathbf{X}}{\partial s^2}\Big/\left|\frac{\partial^2\mathbf{X}}{\partial s^2}\right|\right) - \mathbf{F}, \tag{4}$$

where s is the Lagrangian coordinate along the membrane length and $\mathbf{X} = [X(s,t), Y(s,t)]$ is the position. $\kappa = |\partial^2\mathbf{X}/\partial s^2|$ is the instantaneous membrane curvature and κ_0 is the initial membrane curvature. ϕ is the stretching coefficient of the capsule, γ is the bending coefficient, and ρ_1 denotes the additional boundary density. Note that the surrounding fluid density is subtracted from ρ_1 and that the actual capsule boundary density is $\rho_1 + h\rho_0$, where ρ_0 is the fluid density and h is the capsule thickness. The last term $\mathbf{F}$ represents the Lagrangian forcing acting on the capsule due to the surrounding fluid.

We treated the fluid density ρ_0, the half-channel height H, and the centerline velocity U_m as the characteristic density, length, and velocity, respectively. Thus we introduced the following characteristic scales: H/U_m for the time, $\rho_0\mathrm{H}$ for the boundary mass, $\rho_0 U_m^2$ for the pressure as well as the Lagrangian forcing $\mathbf{F}$, $\rho_0 U_m^2/\mathrm{H}$ for the Eulerian forcing $\mathbf{f}$, $\rho_0 U_m^2\mathrm{H}$ for the stretching coefficient ϕ, and $\rho_0 U_m^2/\mathrm{H}$ for the bending coefficient γ. For convenience, in the remainder of this paper the dimensionless quantities are written in the same form as their dimensional counterparts. After nondimensionalization, Eqs. (2) and (4) take the following dimensionless forms:

$$\frac{\partial\mathbf{u}}{\partial t} + \mathbf{u}\cdot\nabla\mathbf{u} = -\nabla p + \frac{1}{\mathrm{Re}}\nabla^2\mathbf{u} + \mathbf{f}, \tag{5}$$

$$\rho\frac{\partial^2\mathbf{X}}{\partial t^2} = \frac{\partial}{\partial s}\left(\phi\left(\left|\frac{\partial\mathbf{X}}{\partial s}\right| - 1\right)\frac{\partial\mathbf{X}}{\partial s}\Big/\left|\frac{\partial\mathbf{X}}{\partial s}\right|\right) - \frac{\partial^2}{\partial s^2}\left(\gamma\,(\kappa-\kappa_0)\frac{\partial^2\mathbf{X}}{\partial s^2}\Big/\left|\frac{\partial^2\mathbf{X}}{\partial s^2}\right|\right) - \mathbf{F}, \tag{6}$$

where $\mathrm{Re} = \rho_0 U_m\mathrm{H}/\mu$ and $\rho = \rho_1/\rho_0\mathrm{H}$.

Since the fluid and the structure are coupled through the membrane or the immersed boundary (IB) of the capsule, the Lagrangian forcing can be calculated along the IB by using the feedback law

$$\mathbf{F} = \alpha\int_0^t(\mathbf{U}_{\mathrm{ib}} - \mathbf{U})dt + \beta(\mathbf{U}_{\mathrm{ib}} - \mathbf{U}), \tag{7}$$

where $\mathbf{U}_{\mathrm{ib}}$ is the fluid velocity calculated with interpolation at the IB and $\mathbf{U}$ is the velocity of the capsule calculated with $\mathbf{U} = d\mathbf{X}/dt$. The first term of the forcing in Eq. (7) connects the fluid closely to the surface and the second term annihilates the

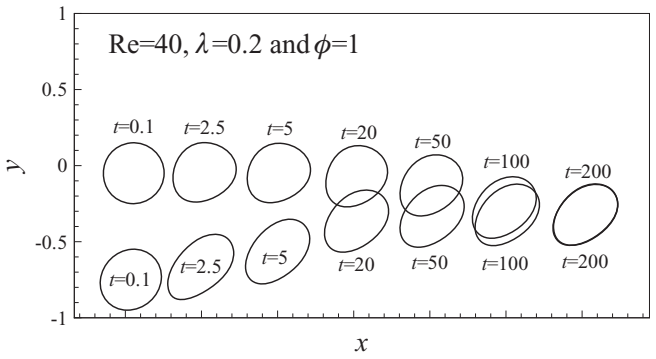

FIG. 2. Migration of the capsule for two different initial lateral positions ($y_0 = -0.05$ and -0.75) in a Poiseuille flow at Re $= 40$, $\lambda = 0.2$, and $\phi = 1$.

difference in the velocity. In other words, this interaction force approximates the no-slip boundary condition on the moving surface. Increasing the values of α and β results in a more accurate interaction force ($\alpha = -10^5$ and $\beta = -10$), which is shownin Table I [24].

The Lagrangian and Eulerian variables were transformed by using the regularized delta function δ. We used the smoothed approximation of the Dirac delta function to interpolate the velocity and momentum forcing between the Eulerian and Lagrangian coordinate systems. For example, the velocity is spread across the immersed boundary with the following equation:

$$\mathbf{U}_{\mathrm{ib}}(s,t) = \int_{\Omega} \mathbf{u}(\mathbf{x},t)\delta(\mathbf{X}(s,t) - \mathbf{x})\, d\mathbf{x}. \tag{8}$$

Here, we used the four-point regularized delta function discussed by Shin *et al.* [24]. Also the Lagrangian forcing was spread to the nearby Eulerian grids by using a similar equation

$$\mathbf{f}(\mathbf{x},t) = \int_{\Gamma} \mathbf{F}(s,t)\delta(\mathbf{x} - \mathbf{X}(s,t))ds. \tag{9}$$

Details regarding the numerical procedure can be found in Shin and Sung [22].

III. RESULTS AND DISCUSSION

The inertial migration of a two-dimensional elastic capsule in a Poiseuille flow was examined by varying the initial lateral position (y_0), Reynolds number, capsule-to-channel size ratio (λ), membrane stretching coefficient (ϕ), and membrane bending coefficient (γ). The bending coefficient γ was assumed to be the ratio of the stretching coefficient to the bending coefficient $\gamma/\phi = 1 \times 10^{-5}$ and the additional boundary density was set at $\rho = 0.01$ by default unless otherwise stated. The computational domain in the y direction ranges from -1 to 1, that is, the channel height is 2. This geometry is symmetrical, so we only considered the migration of the capsule released below the centerline of the channel in the range $-1 \leqslant y_0 \leqslant 0$. As mentioned above, the intercapsule distance (or channel length) was set at L $= 8$. First, the effects of varying the initial lateral position were examined for Re $=$ 40, $\lambda = 0.2$, and $\phi = 1$. The migration of the capsule for two different initial conditions ($y_0 = -0.05$ and -0.75) is shown in Fig. 2. After the capsule is released, it deforms due to the hydrodynamic stresses, and aligns itself at an angle with the direction of the flow. Larger shear stresses are imposed close to the wall, so the deformation of the capsule with $y_0 = -0.75$ is greater and it is more aligned with the flow than that with $y_0 = -0.05$; a different initial lateral position results in different initial behavior. However, as time passes, the two capsules migrate toward the same lateral position and finally attain the same shape and position near $t = 200$.

TABLE I. Comparison of the lateral position, lateral velocity, and slip velocity at $t = 150$ for different computational parameters (α and β) at Re $= 40$, $\lambda = 0.2$, $\phi = 1$, and $y_0 = -0.75$.

	y at $t = 150$	v at $t = 150$	u_{slip} at $t = 150$
$\alpha = -10^5$ and $\beta = -10$	-0.31758	9.81×10^{-5}	0.0369
$\alpha = -10^4$ and $\beta = -10$	-0.31746	9.89×10^{-5}	0.0369
$\alpha = -10^5$ and $\beta = -1$	-0.31758	9.80×10^{-5}	0.0369

Figure 3 shows the evolutions of the lateral position y, lateral velocity v, and slip velocity u_{slip} for $y_0 = 0, -0.05, -0.2, -0.6$, and -0.75. The slip velocity is the relative motion between the fluid and the capsule, and is obtained by subtracting the capsule velocity from the fluid velocity at the location of the capsule centroid in the undisturbed flow. As shown in Fig. 3(a), the capsule starting from the center of the channel ($y_0 = 0$) migrates to the centerline due to the hydrodynamic stresses on the capsule imposed symmetrically by the background Poiseuille flow. When the elastic capsule is released at other lateral positions it moves toward other equilibrium positions. Note that the capsule starting near the channel center ($y_0 = -0.05$) does not move toward the centerline but to another equilibrium position. When the capsule is released closer to the wall, the lateral velocity of the capsule is higher and it migrates more quickly to its equilibrium position. The capsule velocity diminishes in the lateral direction as the capsule reaches the equilibrium position in Fig. 3(b). The slip velocity reaches its maximum value during the initial transient motion and then converges to a steady state, as shown in Fig. 3(c). When the capsule is released closer to the wall, a higher slip velocity is obtained during the initial motion because the viscous shear stress near the bottom wall delays capsule motion. In Fig. 3(d), plots of the lateral velocity as a function of the lateral position are presented for various initial positions. During the initial transient motion, a positive lateral velocity is observed regardless of the initial lateral position. After the initial transient motion, a negative (positive) lateral velocity is generated for $y_0 = -0.05$ and -0.2 ($y_0 = -0.6$ and -0.75) toward the equilibrium position. The lateral velocity, as well as the slip velocity, is an order of magnitude lower than the fluid velocity (or the capsule velocity in the x direction).

In Fig. 4, the velocity vectors are shown at three points in time during the migration of the capsule for two different initial positions. The vectors were obtained by subtracting the x velocity of the capsule centroid from the fluid velocity. In Fig. 4(a), the capsule migrates toward the bottom wall for $y_0 = -0.05$. This phenomenon can be explained by using the Bernoulli equation. At $t = 20$, the relative velocity above the

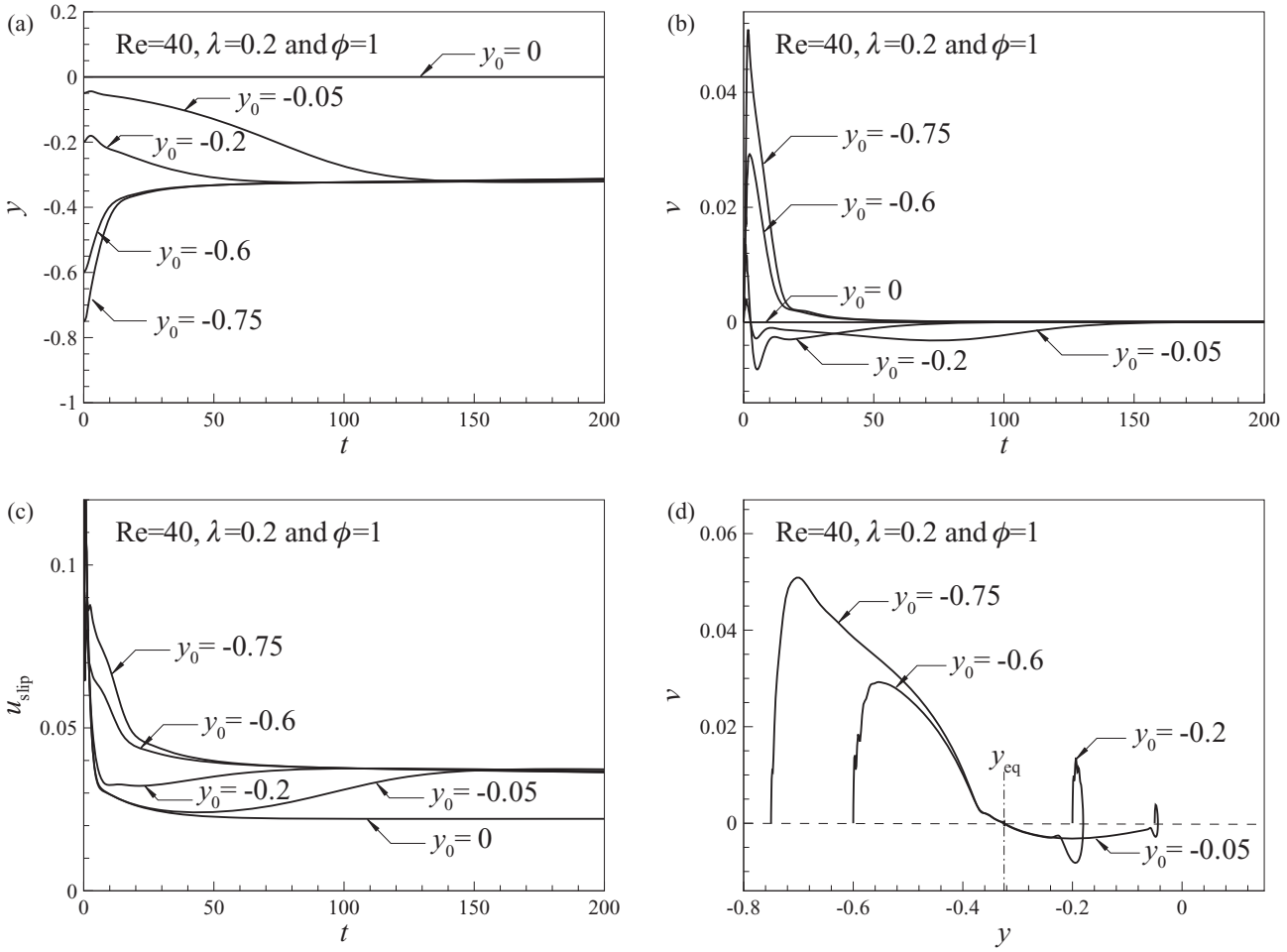

FIG. 3. Variations with time of (a) the lateral position y, (b) the lateral velocity v, (c) the slip velocity, and (d) the lateral velocity versus the lateral position for the elastic capsule in a Poiseuille flow starting with five different initial conditions y_0 at Re $= 40$, $\lambda = 0.2$, and $\phi = 1$.

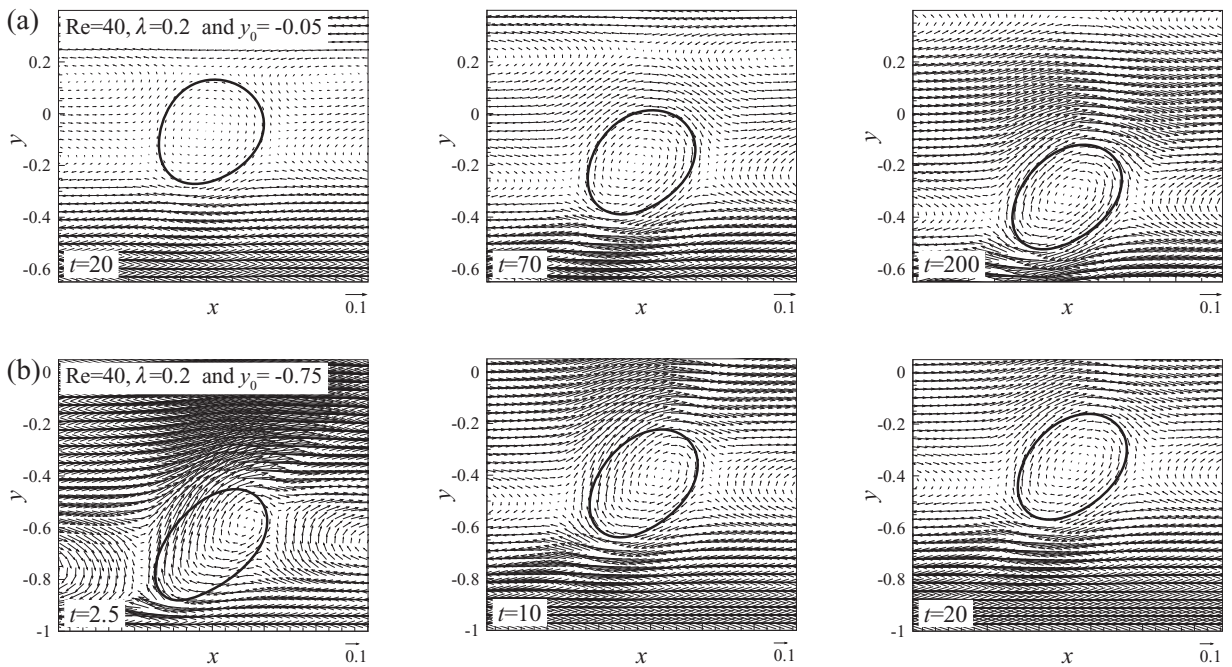

FIG. 4. Velocity vectors (fluid velocity minus x velocity of the capsule center of mass) at three points in time during the migration of the capsule (a) $y_0 = -0.05$ and (b) $y_0 = -0.75$.

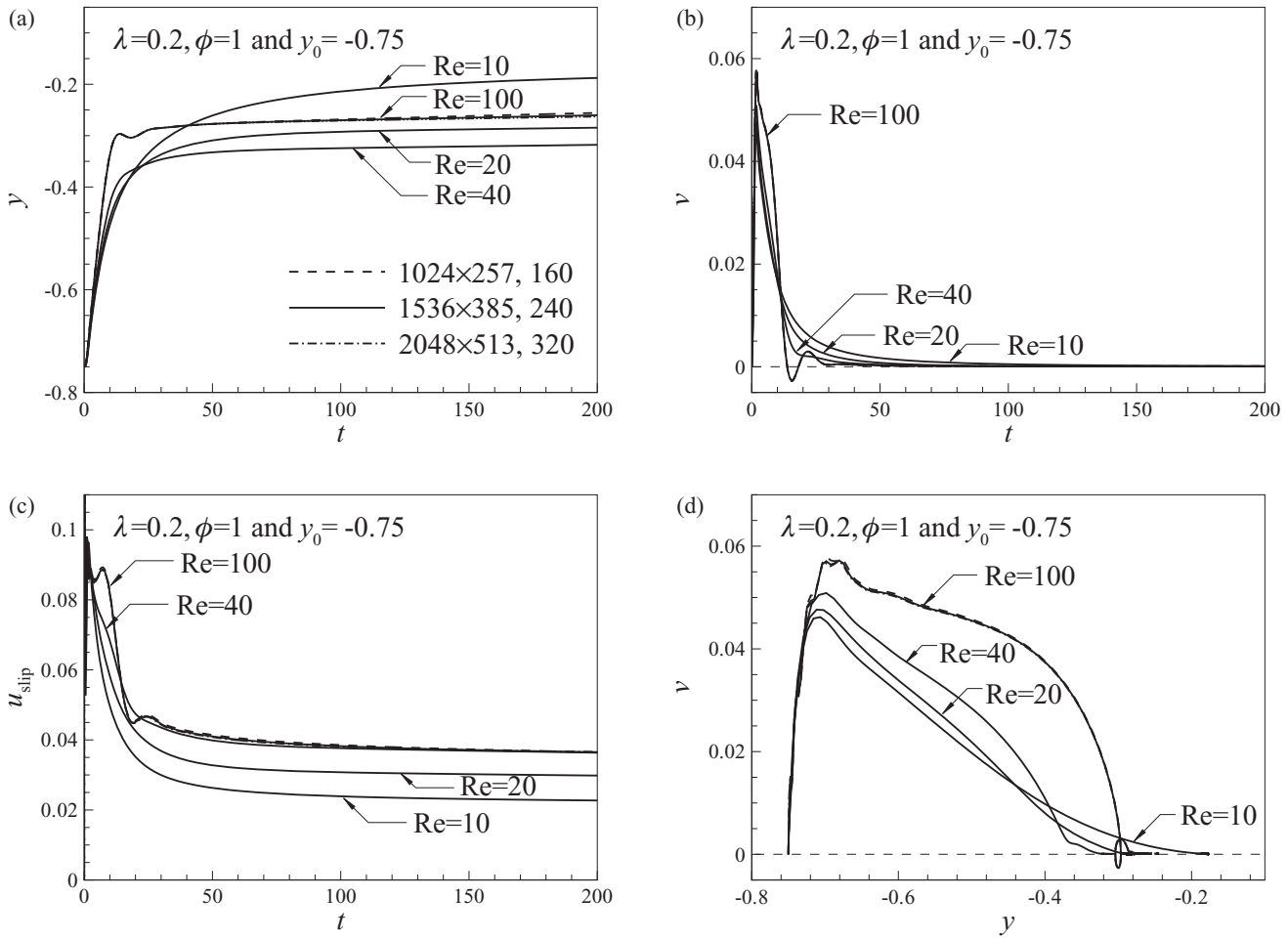

FIG. 5. Variations with time of (a) the lateral position, (b) the lateral velocity, (c) the slip velocity, and (d) the lateral velocity versus the lateral position, for various Reynolds numbers and grid numbers.

capsule is smaller than that below the capsule, which means that the pressure above the capsule is higher than that below the capsule. A negative lift then arises and the capsule moves toward the bottom wall. As time passes, the velocity difference between the top and bottom of the capsule decreases and the negative lift also decreases. A clockwise rotating vortex is generated inside the capsule and the vortex is strengthened as it moves toward the bottom wall. In Fig. 4(b), the capsule is released close to the bottom wall and the interaction between the capsule and wall raises the positive lateral velocity around the capsule at $t = 2.5$. At that time, the center of the clockwise rotating vortex is located above the capsule centroid. When the capsule moves away from the bottom wall, the positive velocity around the capsule is weakened and the center of the vortex is located close to the capsule centroid. The balance between the negative lift given by the Bernoulli equation and the positive lift due to the wall effect results in the specific equilibrium position.

Next, the effects of varying Re on the behavior of the capsule were investigated for $\lambda = 0.2$, $\phi = 1$, and $y_0 = -0.75$. Figure 5 shows the variations with time of the lateral position, lateral velocity, and slip velocity for Re = 10, 20, 40, and 100. Figure 5(a) shows that first the equilibrium position shifts closer to the bottom wall and then toward the channel center as Re increases (see Fig. 8). During the initial transient motion, a higher positive lateral velocity is obtained for higher Re. Transient oscillations of the lateral velocity can be seen in Fig. 5(b), especially for Re = 100. A similar transient oscillation of the deformation of a liquid drop has been reported [25,26]. The transient time required to reach the equilibrium position decreases with increases in Re, as shown in Figs. 5(a) and 5(b). As Re decreases, the slip velocity decreases due to the increase in the viscous force of the fluid flow. The variations for various values of Re of the lateral velocity with the lateral position are presented in Fig. 5(d). The lateral velocity decreases with increases in the lateral distance from the bottom wall, regardless of Re. For lower Re, the region affected by the bottom wall is widened because of the larger viscous force of the fluid flow. Hence, the bottom wall pushes the capsule farther from the wall and the capsule migrates farther from the wall for Re = 10, although the initial positive lateral velocity is smaller than for the other higher Re, as shown in Fig. 5(d). It is expected that, on going to lower Re, the capsule will move even further from the wall until it reaches the center of the channel for very low Re [see Fig. 16(a)]. The sensitivities of the Eulerian and Lagrangian resolutions

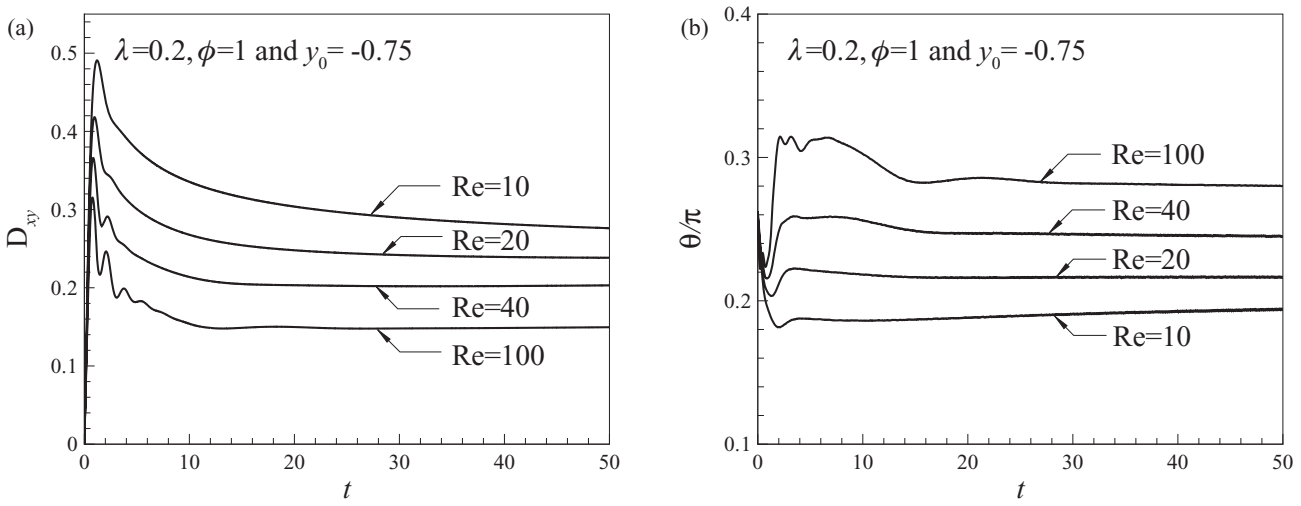

FIG. 6. Variations with time of (a) the Taylor deformation parameter and (b) the inclination angle (with respect to the x axis) for various Reynolds numbers.

were tested by selecting three different resolutions for Re = 100: (i) 1024 × 257 Eulerian grids and 160 Lagrangian grids; (ii) 1536 × 385 Eulerian grids and 240 Lagrangian grids; (iii) 2048 × 513 Eulerian grids and 320 Lagrangian grids. As can be seen in Fig. 5, no significant difference was observed. In the present study, 1536 × 385 Eulerian grids and 240 Lagrangian grids were used.

The effects of varying Re on capsule deformation were also studied. Figure 6 shows the initial variations with time of the Taylor deformation parameter D_{xy} and the inclination angle θ for various Re. The Taylor deformation parameter is defined as $D_{xy} = (L_A - L_B)/(L_A + L_B)$, where L_A and L_B are the maximum and minimum radii, respectively, of the deformed capsule. The inclination angle is the angle between L_A and the x axis. Since the viscosity effects are larger for lower Re, the deformation of the capsule is greater and it is better aligned with the direction of the flow. As a result, D_{xy} increases and θ/π decreases for lower Re.

We examined the migration of a capsule starting near the center ($y_0 = -0.15$) for various Reynolds numbers. The variations of the lateral position are shown in Fig. 7(a) for two different initial positions. The capsules with $y_0 = -0.15$ and $y_0 = -0.75$ move faster to the equilibrium position as Re increases. Transient oscillations of the lateral velocity can be seen in Figs. 7(b) and 7(d). As for $y_0 = -0.75$, a higher positive lateral velocity is obtained during the initial transient motion for a higher Re. After the initial transient motion, however, a negative lateral velocity is observed until the capsule reaches the equilibrium position. At Re = 40, the negative lateral velocity is higher than for other values of Re, as shown in Figs. 7(b) and 7(d), in accordance with the equilibrium position. The slip velocity increases with increases in Re due to the decreases in viscous stress, as shown in Fig. 7(c). The variations of the equilibrium position y_{eq} of the capsule with the capsule-to-channel size ratio λ and Re are presented in Fig. 8. The equilibrium position is defined as the distance between the channel centerline and the capsule centroid. There is a peak in the equilibrium position near Re = 30 for λ = 0.1 and this peak shifts to higher Re for larger λ. The equilibrium position moves up toward the center of the channel ($y_{eq} = 0$) with increasing λ. The capsule migrates to the centerline of the channel, regardless of Re, especially for λ = 0.4.

During the migration, the capsule not only moves toward the equilibrium position, but also its membrane rotates in a clockwise direction as it becomes stressed in the fluid flow [27]. After the capsule reaches the equilibrium position, its shape becomes constant and its membrane rotates with a frequency f. This tank-treading motion is presented in Fig. 9(a) as a series of capsule contours for Re = 100, λ = 0.2, and ϕ = 1. The small square symbols indicate the same Lagrangian point on the membrane, and thus clearly show the clockwise rotating motion. The Strouhal number for tank-treading motion St = (Hf)/U_m is shown in Fig. 9(b) for various size ratios and Reynolds numbers. The variation of St is similar to that of the equilibrium position shown in Fig. 8. As mentioned in Fig. 4(a), a clockwise rotating vortex is generated inside the capsule and the vortex is strengthened as the capsule approaches the bottom wall. When the equilibrium position is closer to the wall, the capsule is affected by larger shear stresses and it rotates faster. For λ = 0.2, the capsule with Re = 40 migrates closer to the bottom wall and a larger clockwise vortex is generated than that with other Reynolds numbers. Similarly, for λ = 0.4, the capsule moves toward the centerline and its membrane no longer rotates due to the symmetrical hydrodynamic stresses.

The effects of varying the capsule-to-channel size ratio on the migration of the capsule were scrutinized for Re = 40, ϕ = 1, and $y_0 = -0.55$. Figure 10 shows the variations of the lateral position, lateral velocity, and slip velocity for various size ratios λ = 0.1, 0.2, 0.3, and 0.4. For larger λ, the capsule moves more strongly toward the center of the channel, as shown in Fig. 10(a). During the initial transient motion, a higher positive lateral velocity is obtained for larger λ, as shown in Fig. 10(b). Figure 11 shows the fluid velocity vectors at three points in time for two different size ratios. The fluid velocity below the capsule is lower due to the no-slip

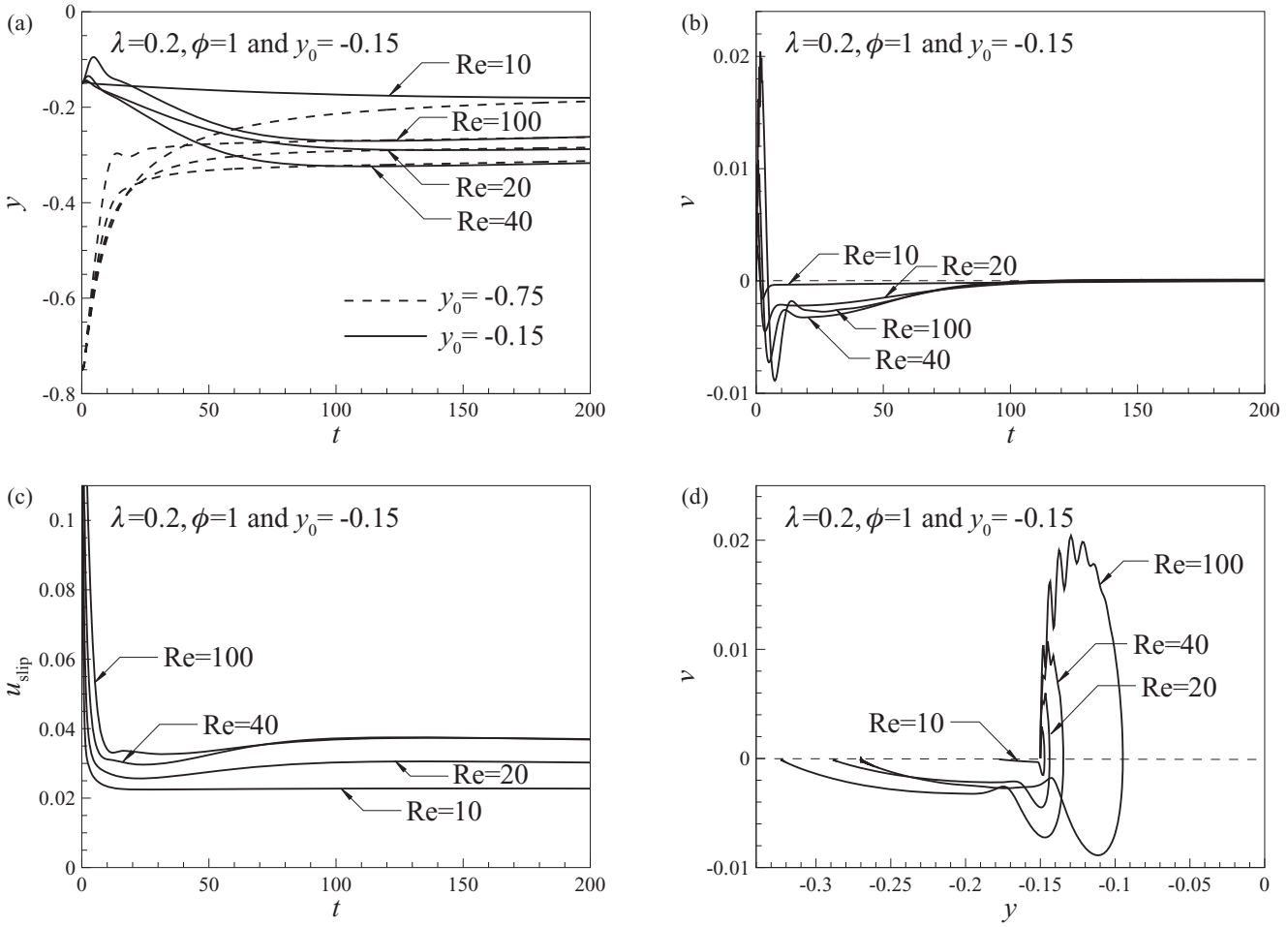

FIG. 7. Variations with time of (a) the lateral position, (b) the lateral velocity, (c) the slip velocity, and (d) the lateral velocity versus the lateral position for various Reynolds numbers.

condition of the bottom wall. The velocity difference between the bottom and top of the capsule increases with increasing λ, as shown in Fig. 11. A larger velocity difference generates a larger positive lift according to the Bernoulli equation. In addition, the bottom part of a capsule with a larger size ratio is closer to the bottom wall for the same lateral position of the capsule centroid. Hence, the capsule with a larger size ratio is influenced more by the wall and a larger positive lateral velocity is generated, as shown in Fig. 10(d). The slip velocity in Fig. 10(c) also increases with the size ratio because of the larger hydrodynamic effect of the bottom wall. As a result, the capsule with $\lambda = 0.4$ migrates more strongly toward the centerline than that with $\lambda = 0.2$, as shown in Fig. 11. At $t = 200$, the capsule with $\lambda = 0.4$ reaches the centerline and its shape becomes that of a parachute due to the hydrodynamic stresses of the background Poiseuille flow [28,29].

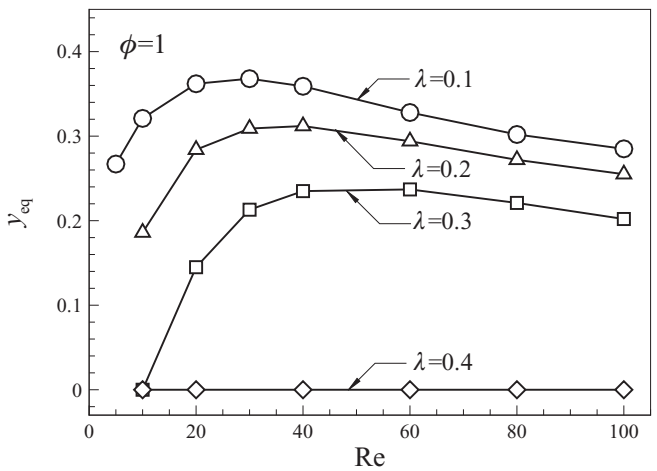

FIG. 8. Equilibrium positions of the elastic capsule for $\lambda = 0.1$, 0.2, 0.3, and 0.4, for the range Re = 5–100.

The effects of varying the membrane stretching coefficient ϕ and bending coefficient γ on the equilibrium position of the capsule are displayed in Fig. 12. As ϕ increases, the equilibrium position shifts toward the bottom wall ($y_{eq} = 1$). There is a peak in the equilibrium position near Re = 40 for $\phi = 1$ and this peak moves to Re = 30 for $\phi = 10$ and 100. The equilibrium position shifts toward the bottom wall for larger γ in Fig. 12(b). Figure 13 depicts the variations of the lateral position, the lateral velocity, and the slip velocity for various membrane stretching coefficients, $\phi = 1$, 10, and 100; in this figure, Re = 10, $\lambda = 0.2$, and $\gamma = 10^{-5}$. For smaller ϕ, a larger positive lateral velocity is generated, as shown in Figs. 13(b) and 13(d). Accordingly, as the membrane

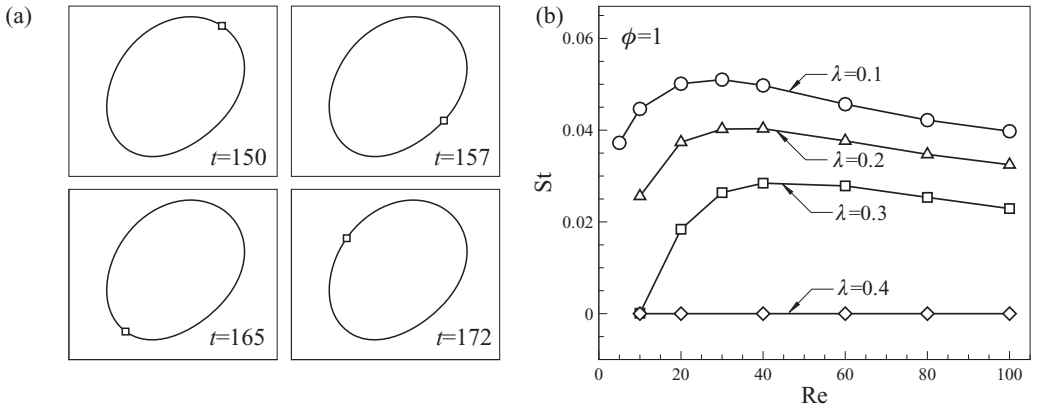

FIG. 9. (a) Tank-treading motion for Re = 100, λ = 0.2, and $\phi = 1$. (b) The variation of the Strouhal number with Re for various values of the size ratio λ.

stretching coefficient decreases, the capsule migrates more strongly toward the center, as shown in Fig. 13(a). The slip velocity is smaller for more deformable capsule ($\phi = 1$) in Fig. 13(c) because it exhibits the less resistance to the flow. Figure 14 depicts the variations of the lateral position, the lateral velocity, and the slip velocity for various membrane bending coefficients $\gamma = 10^{-5}, 10^{-4}$, and 10^{-3} at Re = 40, λ = 0.2, and $\phi = 10$. For smaller γ, the slip velocity decreases and a higher positive lateral velocity is obtained in Fig. 14.

The variation of the Taylor deformation parameter D_{xy} is presented in Fig. 15(a) for three different membrane stretching coefficients ϕ. The initial peak of the deformation

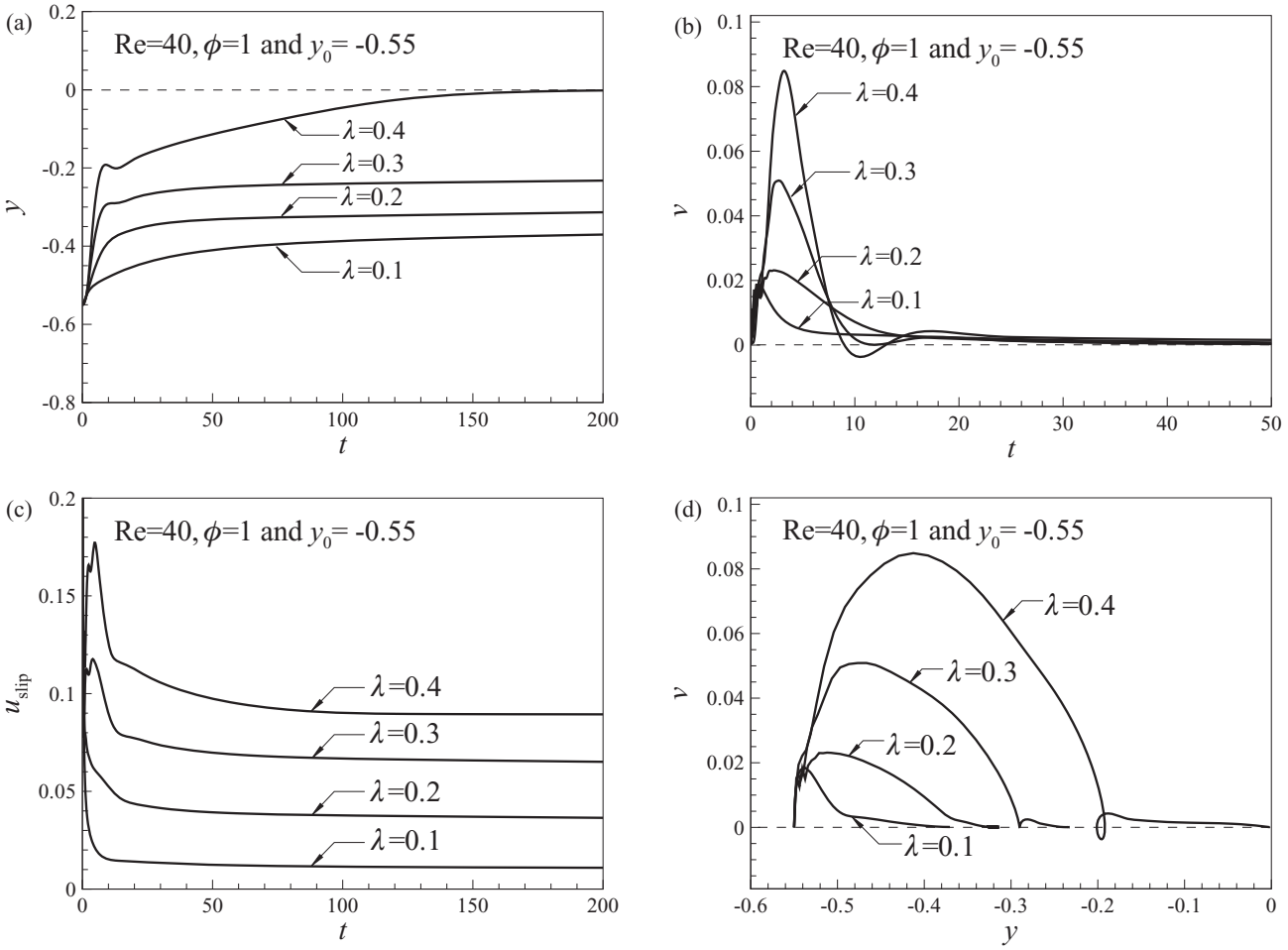

FIG. 10. Variations with time of (a) the lateral position, (b) the lateral velocity, (c) the slip velocity, and (d) the lateral velocity versus the lateral position for various capsule-to-channel size ratios λ.

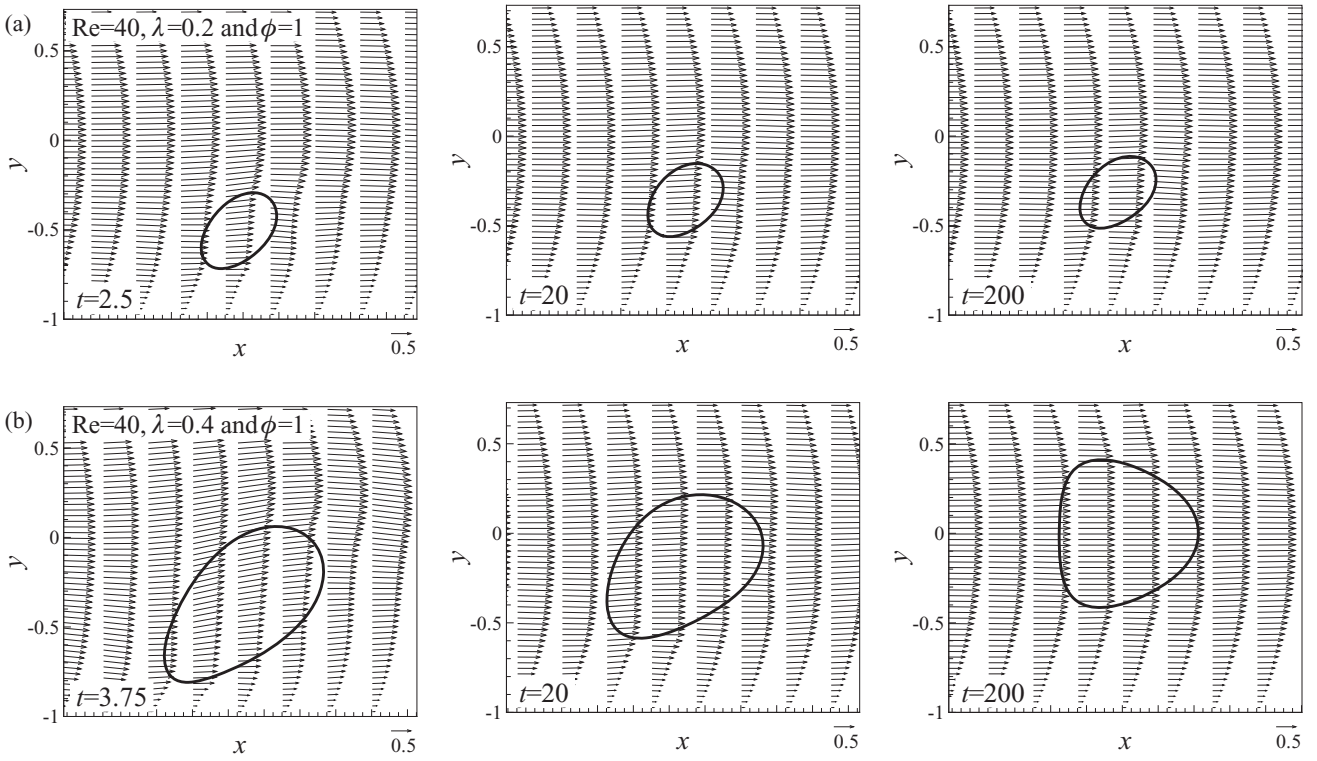

FIG. 11. Fluid velocity vectors at three points in time during the migration of capsules with $y_0 = -0.55$. (a) $\lambda = 0.2$ and (b) $\lambda = 0.4$.

rapidly rises, and then converges to a steady state. As the membrane stretching coefficient ϕ increases, the deformation of the capsule decreases. Figure 15(b) shows the effect of the bending coefficient γ on D_{xy} . The deformation of the capsule decreases with increasing γ. This variation is similar to that of the equilibrium position shown in Fig. 12(b). These figures show that the deformation of the capsule is closely related with the capsule migration. The deformation of the capsule influences the balance of the hydrodynamic forces, particularly the viscous shear and inertia forces, and finally determines the specific equilibrium position. This phenomenon might be useful in biological applications, such as the separation of cells that have similar size but different membrane elasticity.

The effects of varying the size ratio and Re on the lateral velocity were scrutinized for $\phi = 10$ and $y_0 = -0.65$. The lateral velocity is depicted as a function of the lateral position in Figs. 16(a), 16(b), and 16(c) for Re = 1, 10, and 100, respectively. The wall pushes the capsule farther from the wall for lower Re, as mentioned above, and the capsule for Re = 1 moves more strongly until it reaches the centerline regardless of the size ratio [28,29]. For Re = 10, the variations

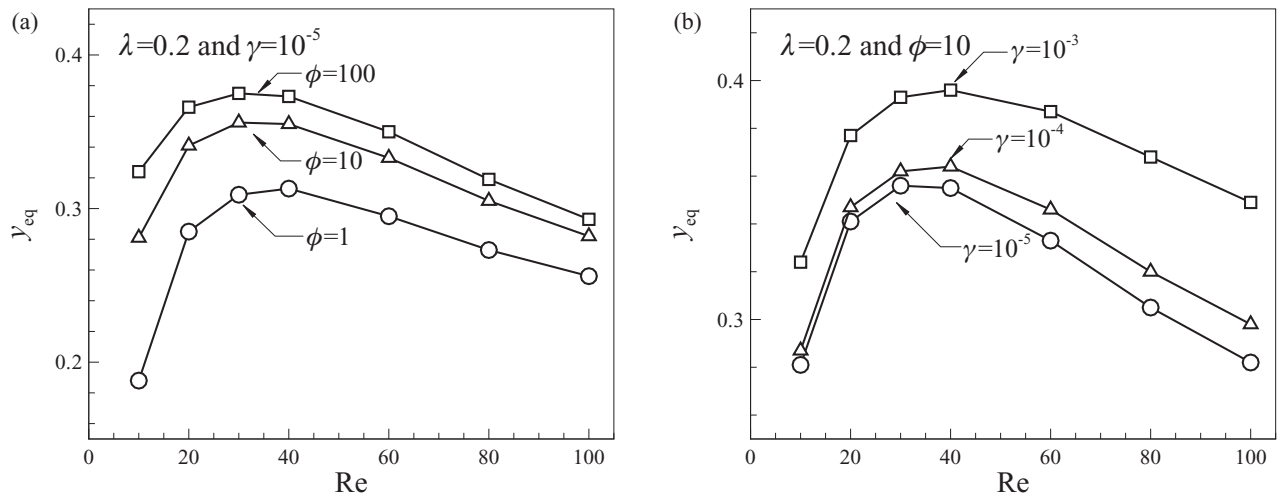

FIG. 12. Equilibrium positions for various membrane stretching coefficients ϕ and bending coefficientsγ for the range Re = 10–100.

of the lateral velocity are similar to those for Re = 1, though the equilibrium positions are different to those for Re = 1. On the other hand, the variation of the lateral velocity for Re = 100 is very different from those for Re = 1 and 10 due to the larger inertial effect. Figures 16(d), 16(e), and 16(f) show the variations of the lateral velocity as functions of λ^3 keeping the lateral position constant. The lateral velocity increases linearly with λ^3 for Re = 1 and 10. These results are in good agreement with previous analytical predictions [20,30]. Note that the inertial effect was not considered in these previous studies. As Re increases, a deviation is observed from the linear dependence of v on λ^3 for Re = 100, which might be due to the effects of fluid inertia on capsule migration.

During migration in a Poiseuille flow, the capsule experiences two lift forces perpendicular to the flow direction: one generated by the shear gradient effect and the other by the wall effect. The negative lift toward the bottom wall is generated by the shear gradient in the Poiseuille flow. The x velocity of the capsule centroid u_c is obtained by subtracting the slip velocity u_{slip} from the fluid velocity at the location of the capsule centroid in the undisturbed flow, as shown in Eq. (1),

$$u_c = \left(1 - y_c^2\right) - u_{\text{slip}}. \tag{10}$$

The fluid velocities at the top and bottom of the capsule can be obtained as follows

$$\begin{aligned} u_{\text{top}} &= (1 - (-y_c + \lambda)^2), \\ u_{\text{bottom}} &= (1 - (-y_c - \lambda)^2) \quad \text{for } 0 \leqslant y_c \leqslant 1. \end{aligned} \tag{11}$$

Then, the relative velocities between the fluid and capsule at the top and bottom can be calculated as follows:

$$\begin{aligned} u_{\text{top}}^{\text{rel}} &= u_{\text{top}} - u_c = (2\lambda y_c - \lambda^2) + u_{\text{slip}} \\ u_{\text{bottom}}^{\text{rel}} &= u_c - u_{\text{bottom}}^{\text{rel}} = (2\lambda y_c + \lambda^2) - u_{\text{slip}}. \end{aligned} \tag{12}$$

For simplicity, we can neglect the slip velocity u_{slip} because it is relatively small. The relative velocity at the top of the capsule is always smaller than that at the bottom of the capsule, which means that the pressure at the top of the capsule is higher than that at the bottom of the capsule. The negative lift force arises around the capsule due to the Poiseuille flow velocity profile.

On the other hand, a positive lift force toward the center of the channel develops due to the no-slip condition of the bottom wall. When the capsule is closer to the wall, the fluid velocity profile is changed by the larger shear stress of the wall and a higher pressure is generated below the capsule. As

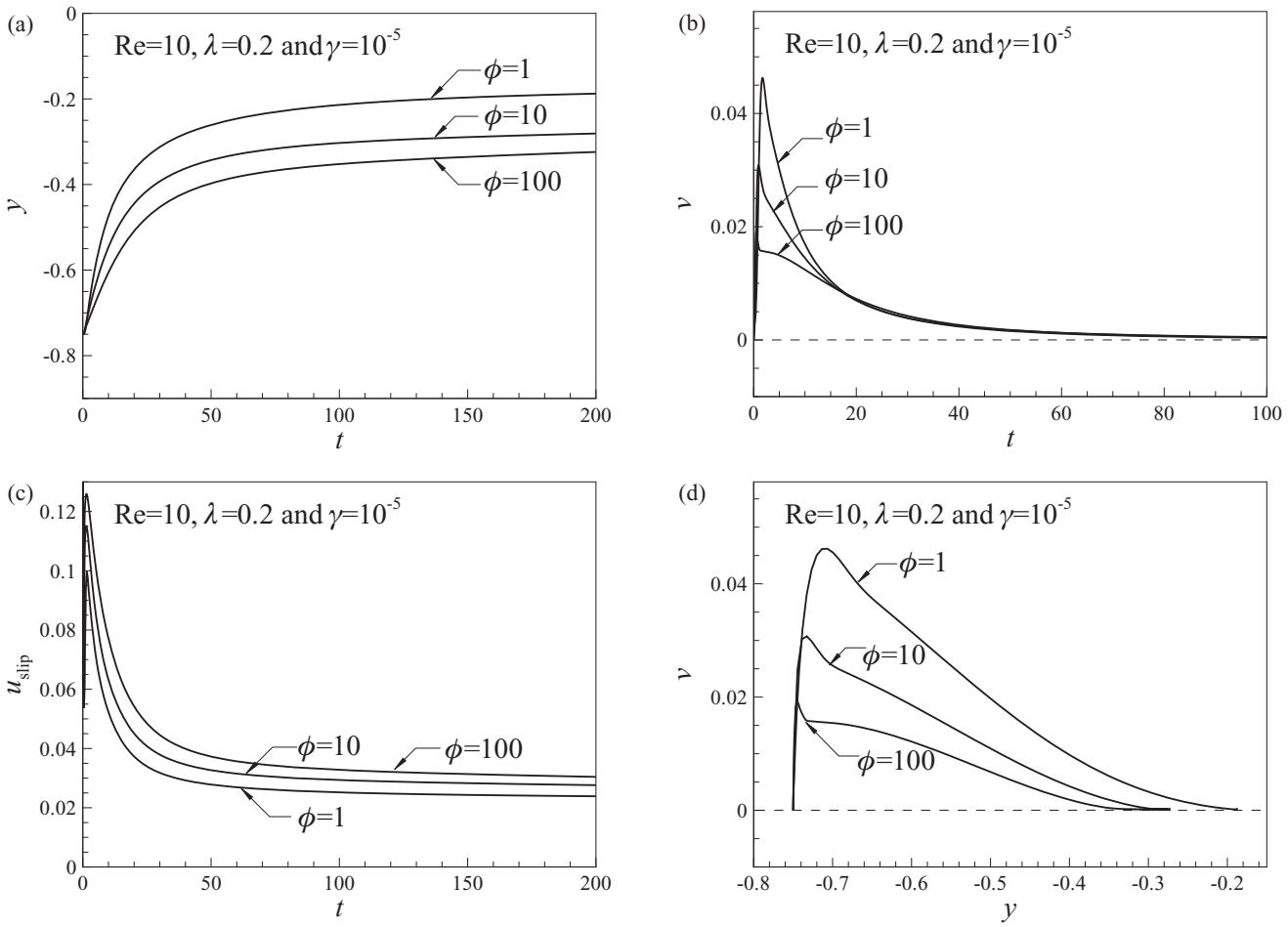

FIG. 13. Variations with time of (a) the lateral position, (b) the lateral velocity, (c) the slip velocity, and (d) the lateral velocity versus the lateral position for various values of ϕ.

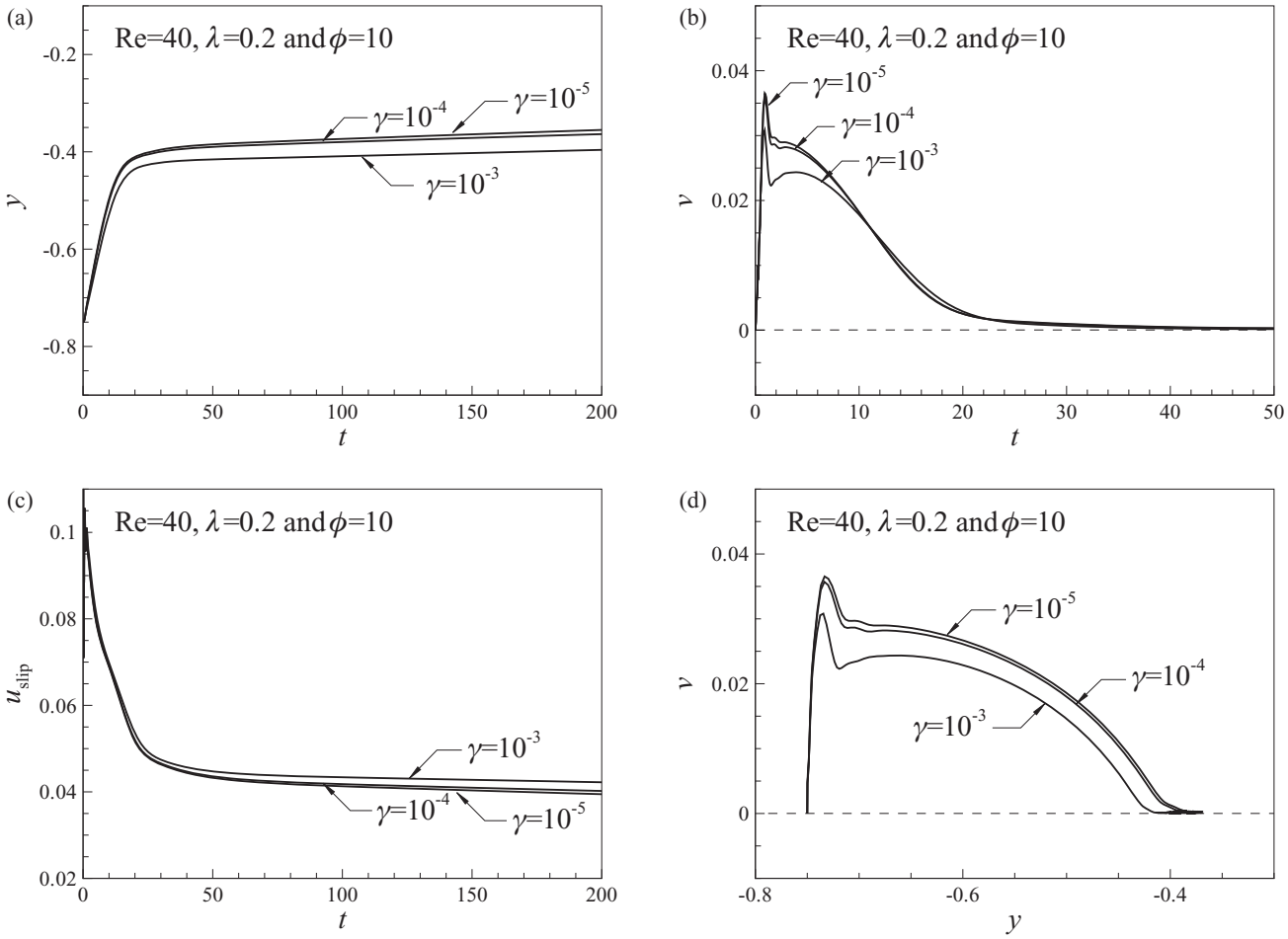

FIG. 14. Variations with time of (a) the lateral position, (b) the lateral velocity, (c) the slip velocity, and (d) the lateral velocity versus the lateral position for various values of γ.

Re increases, a smaller wall effect generates a smaller positive lift force and then the equilibrium position shifts toward the bottom wall. As Re increases further, the fluid velocity profile becomes flatter and the velocity difference between the top and bottom of the capsule decreases. Hence, for much higher Re, the negative lift force due to the shear gradient effect decreases and the equilibrium position shifts toward the channel center.

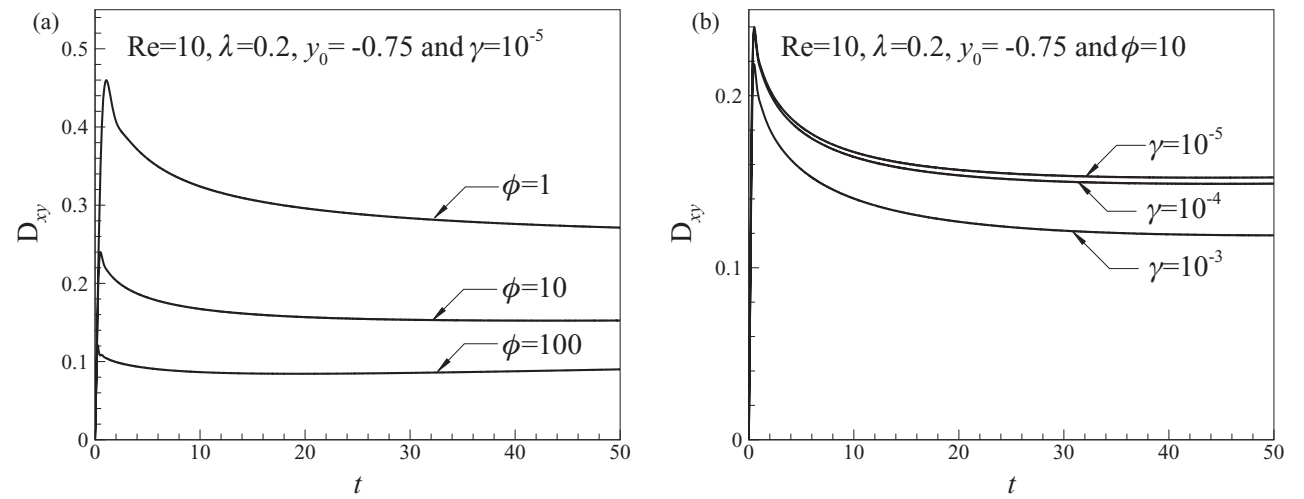

FIG. 15. Variation of the Taylor deformation parameter D_{xy} for various values of (a) membrane stretching coefficients ϕ and (b) bending coefficients γ at $\mathrm{Re} = 10$, $\lambda = 0.2$, and $y_0 = -0.75$.

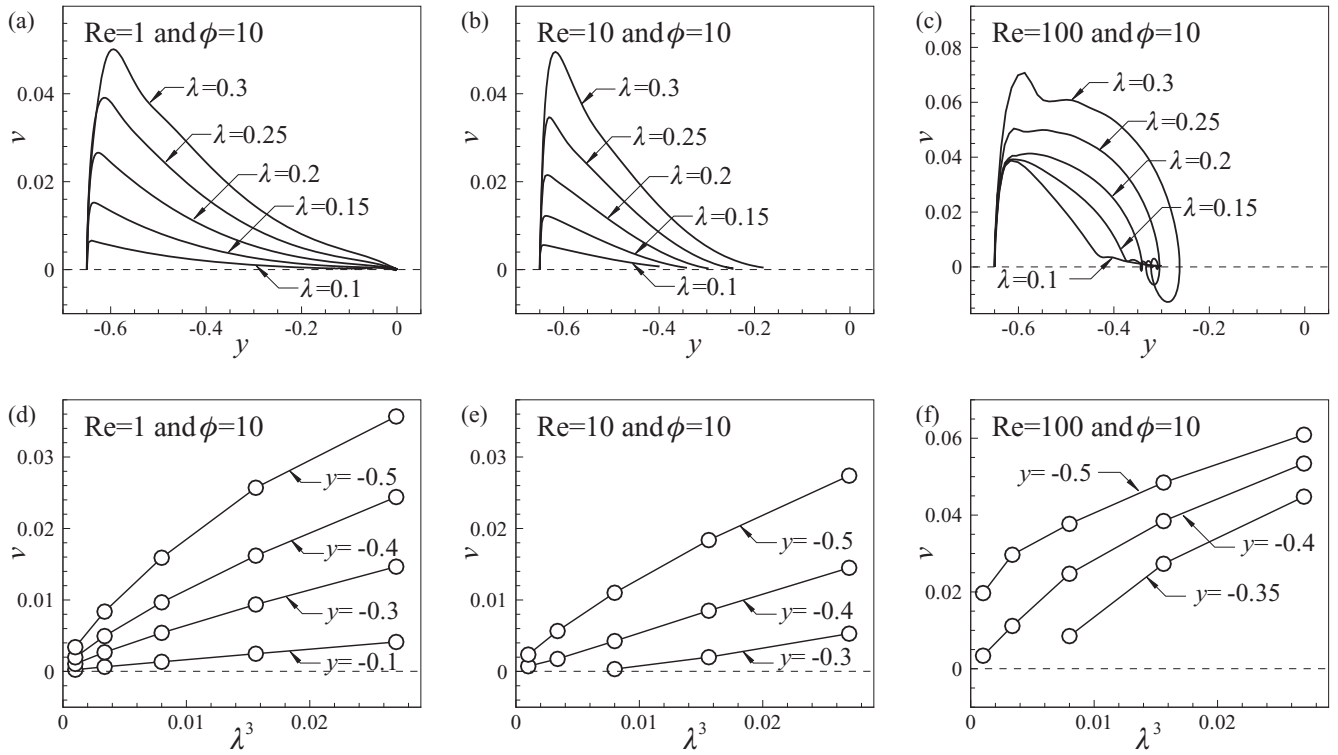

FIG. 16. Plots of the lateral velocity as a function of the lateral position for (a) Re = 1, (b) Re = 10, and (c) Re = 100, and the variations of the lateral velocity with the capsule-to-channel size ratio λ for (d) Re = 1, (e) Re = 10, and (f) Re = 100.

IV. CONCLUSION

The inertial migration of an elastic capsule in a Poiseuille flow has been studied numerically by using the immersed boundary method. The behavior of the capsule is affected by various parameters, particularly the initial lateral position (y_0), Re, the capsule-to-channel size ratio (λ), the membrane stretching coefficient (ϕ), and the membrane bending coefficient (γ). A different initial lateral position of the capsule results in different initial behavior. When the capsule is released closer to the wall, the lateral velocity is higher and the capsule migrates more quickly toward the equilibrium position. Larger shear stresses are imposed closer to the wall, so the deformation of the capsule is larger and a higher slip velocity is observed. However, as time passes, the capsule migrates to the same equilibrium position regardless of the initial lateral position. The effects of varying Re on the capsule behavior were also studied. As Re increases, a higher positive lateral velocity is obtained during the initial transient motion and less transient time is required to reach the equilibrium position. Since the viscosity effects are smaller for higher Re, the capsule deforms less, is less aligned with the direction of the fluid flow, and the slip velocity increases. A change in the Reynolds number affects the equilibrium position by changing the fluid velocity profile and the strength of the shear stress near the wall. As Re increases, the size of the region that is affected by the wall decreases because the viscous force of the fluid is weaker. For higher Re, the negative lift force due to the shear gradient decreases because the fluid velocity profile is flatter and the velocity difference between the top and bottom of the capsule decreases. The balance between the wall effect and the shear gradient effect determines the equilibrium position. As a result, the equilibrium position first shifts closer to the bottom wall and then to the channel center, as Re increases. There is a peak in the equilibrium position near Re = 30 for the capsule-to-channel size ratio λ = 0.1 and the peak shifts to higher Re as the capsule-to-channel size ratio increases. As the size ratio λ increases, the velocity difference between the bottom and the top of the capsule becomes larger and the capsule is influenced more by the wall for the same lateral position of the capsule centroid. As a result, a higher positive lateral velocity is generated and the equilibrium approaches the upper centerline for larger λ. The membrane stretching coefficient (ϕ) and bending coefficient (γ) directly influence the deformation of the capsule. For larger ϕ and γ, the capsule deforms less and the inclination angle is larger. Capsule deformation affects the balance between the viscous shear force and inertia force, and changes the specific equilibrium position. As ϕ and γ increase, a lower positive lateral velocity is generated around the capsule and the equilibrium position moves toward the wall. During the migration of the capsule, the capsule membrane rotates due to the shear stresses of fluid flow. This tank-treading motion is closely related to the equilibrium position. As the equilibrium position moves closer to the wall, the capsule becomes influenced by the larger shear stresses and then its membrane rotates faster. As a result, the variation of St for the tank-treading motion is proportional to that of the equilibrium position.

ACKNOWLEDGMENTS

This study was supported by the Creative Research Initiatives (Grant No. 2011-0000433) of the National Research Foundation of Korea.

[1] C. Pozrikidis, Ann. Biomed. Eng. **31**, 1194 (2003).
[2] S. V. Marella and H. S. Udaykumar, Phys. Fluids **16**, 244 (2004).
[3] Y. W. Kim and J.Y. Yoo, Lab Chip **9**, 1043 (2009).
[4] W. Lee, H. Amini, H. A. Stone, and D. Di Carlo, PNAS **107**, 22413 (2010).
[5] D. Barthès-Biesel, J. Fluid Mech. **100**, 831 (1980).
[6] P. R. Rao, G. I. Zahalak, and S. P. Sutera, J. Fluid Mech. **270**, 73 (1994).
[7] K. S. Chang and W. L. Olbricht, J. Fluid Mech. **250**, 587 (1993).
[8] A. Walter, H. Rehage, and H. Leonhard, Colloid Polym. Sci. **278**, 169 (2000).
[9] S. Ramanujan and C. Pozrikidis, J. Fluid Mech. **361**, 117 (1998).
[10] Y. Sui, Y. T. Chew, P. Roy, X. B. Chen, and H. T. Low, Phys. Rev. E **75**, 066301 (2007).
[11] Y. Sui, Y. T. Chew, P. Roy, and H. T. Low, J. Comput. Phys. **227**, 6351 (2008).
[12] P. C.-H Chan and L. G. Leal, J. Fluid Mech. **92**, 131 (1979).
[13] S. K. Doddi and P. Bagchi, Int. J. Multiphase Flow **34**, 966 (2008).
[14] G. Ma, J. Hua, and H. Li, Phys. Rev. E **79**, 046710 (2009).
[15] R. D. Jäggi, R. Sandoz, and C. S. Effenhauser, Microfluid Nanofluid **3**, 47 (2007).
[16] D. Di Carlo, Lab Chip **9**, 3038 (2009).
[17] G. Segré and A. Silberberg, Nature (London) **189**, 209 (1961).
[18] E. S. Asmolov, J. Fluid Mech. **381**, 63 (1999).
[19] J. Matas, J. F. Morris, and E. Guazzelli, J. Fluid Mech. **515**, 171 (2004).
[20] B. Chun and A. J. C. Ladd, Phys. Fluids **18**, 031704 (2006).
[21] W.-X. Huang, S. J. Shin, and H. J. Sung, J. Comput. Phys. **226**, 2206 (2007).
[22] S. J. Shin and H. J. Sung, Int. J. Heat Fluid Flow **31**, 942 (2010).
[23] C. Song, S. J. Shin, H. J. Sung, and K.-S. Chang, J. Fluid. Struct. **27**, 438 (2011).
[24] S. J. Shin, W.-X. Huang, and H. J. Sung, Int. J. Numer. Meth. Fluids **58**, 263 (2008).
[25] S. Mortazavi and G. Tryggvason, J. Fluid Mech. **411**, 325 (2000).
[26] J. Lee and C. Pozrikidis, Computers and Fluids **35**, 43 (2006).
[27] M. Kraus, W. Wintz, U. Seifert, and R. Lipowsky, PRL **77**, 3685 (1996).
[28] B. Kaoui, G. H. Ristow, I. Cantat, C. Misbah, and W. Zimmermann, Phys. Rev. E **77**, 021903 (2008).
[29] H. Noguchi and G. Gompper, PNAS **102**, 14159 (2005).
[30] A. Helmy and D. Barthès-Biesel, J. Mec. Theor. Appl. **1**, 859 (1982).